8-25-2017

New concepts for use in low-energy cardiac defibrillation

Kayleigh Wheeler
kmw7139@rit.edu

New concepts for use in low-energy cardiac defibrillation

by

Kayleigh Wheeler

A Thesis Submitted in Partial Fulfillment of the Requirements
for the Degree of Master of Science in Applied and Computational Mathematics
School of Mathematical Sciences, College of Science

Rochester Institute of Technology
Rochester, NY
August 25, 2017

Committee Approval:

R·I·T
College of
SCIENCE

Niels Otani Date

School of Mathematical Sciences

Thesis Advisor

Elizabeth Cherry Date

School of Mathematical Sciences

Committee Member

Laura Munoz Date

School of Mathematical Sciences

Committee Member

Matthew Hoffman Date

School of Mathematical Sciences

Director of Graduate Programs

Abstract

The presence of three-dimensional rotating action potential waves, called scroll waves, in the heart causes ventricular fibrillation. Recently, there has been interest in developing low-energy methods, consisting of applying an electric field to terminate these waves, as a means of defibrillation. The success of these methods often depends on the orientation of the waves. We present computer simulations of a method that applies multiple electrical fields in a hemispherical shell system representative of the ventricles of the heart. Scroll waves in this system persist when the filament (the curve around which the wave rotates) connects the inside and outside surfaces. Our scheme for applying electric fields aims to disconnect these filaments from the surfaces. Once the filaments no longer connect the inside and outside surfaces, they contract and disappear, terminating the scroll wave. Importantly, as opposed to most existing schemes, the idea on which this scheme is based is applicable irrespective of how many scroll waves are present, where they are located, or where they are in their rotation. We discuss the success of this scheme both for different numbers of waves and for different wave orientations and present potential failure mechanisms. The effects of other conditions, such as the stability of the waves and heart geometry, remain to be studied. In the future, the presented low-energy method for termination of scroll waves may be a useful means of cardiac defibrillation.

Contents

I. Introduction

Sudden cardiac arrest (SCA) kills about 350,000 people in the United States each year [1]. One of the main causes of SCA is ventricular fibrillation, defined as a state of unorganized electrical activity in the heart. Many efforts have been made to develop low-energy methods for the termination of this chaotic activity. We develop methods in which a series of electric fields are applied to a heart-like system.

I.1 Physiology of the Heart

The heart consists of four chambers; the left and right atria and the left and right ventricles. The atria pump blood into the ventricles, which in turn pump blood to the rest of the body. Different types of cardiac muscle include atrial, ventricular, excitatory, and conductive [2]. The wall of the ventricles is made of three types of muscle [2]; epicardium (outer), mid-myocardium (middle), and endocardium (inner). All three types contain cardiac muscle cells with varying properties. Cells in the sinus node, located in the atria, fire by themselves, creating an electric signal which starts a heart beat. This pulse then travels through the atria and into the ventricles via the A-V node. Here the pulse is delayed to allow time for the ventricles to fill with blood. The pulse finally travels through the ventricles, carried by Purkinje fibers. Fibers in the cardiac muscle are striated, arranged in lattice work. Individual cells are separated by structures called intercalated discs. Corridors called gap junctions connect the interiors of adjacent cells, allowing the diffusion of intracellular ions between cells, primarily in the fiber direction. This allows action potentials to travel easily between cardiac cells, especially in the fiber direction.

An action potential is a rapid change in membrane potential [2], the difference in electric potentials inside and outside of a cell, which spreads quickly from cell to cell. A cell is said to be polarized when it is in a resting state, having negative membrane potential. The rapid increase of the membrane potential of a cell is called depolarization. In cardiac cells, this happens when the membrane becomes permeable to positively charged sodium ions. These ions flow into the cell, causing an increase in the membrane potential. The sodium channels (the specialized pores through which the sodium ions pass) promptly close. The potassium and calcium channels then open. For some time, the calcium flowing into and potassium flowing out of the cell counteract each other, leaving the cell depolarized for some time (about 0.2 seconds in humans). Once the calcium channels close, the flow of potassium to the extracellular region rapidly decreases the

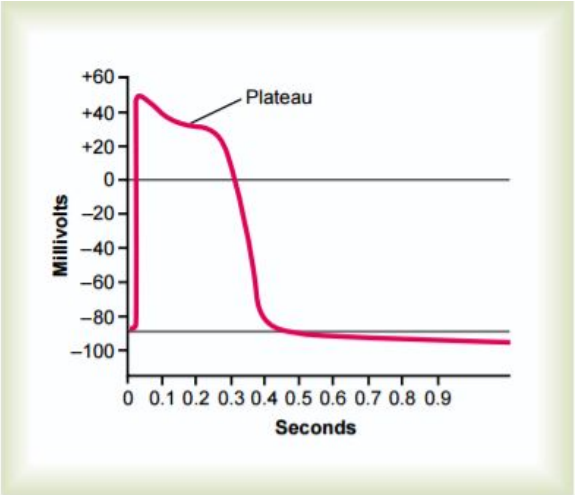

Figure 1: Action potential in a Purkinje heart fiber [2]

potential back to its resting state. This is called repolarization. Hyperpolarization occurs when the membrane potential decreases below the resting state. A simplified action potential cycle can be seen in Figure 1.

Our new defibrillation method requires the application of one or more electric field pulses to the heart. The effect of an electric field applied to cardiac tissue may be described in terms of an electrical circuit, as shown in Figure 2. The corridor in the lower part of the diagram represents the extracellular medium (i.e., the spaces between the cardiac cells). The blocks above this corridor represent cardiac cells. Current injected from the positive electrode passes into the adjacent circuits through the tissue edge (the left boundary of the leftmost cell). It is forced to pass back into the original circuit by the inexcitable block shown as a gap in the tissue. The passing of current into and out of cells causes the hyperpolarization (blue) and depolarization (pink), respectively.

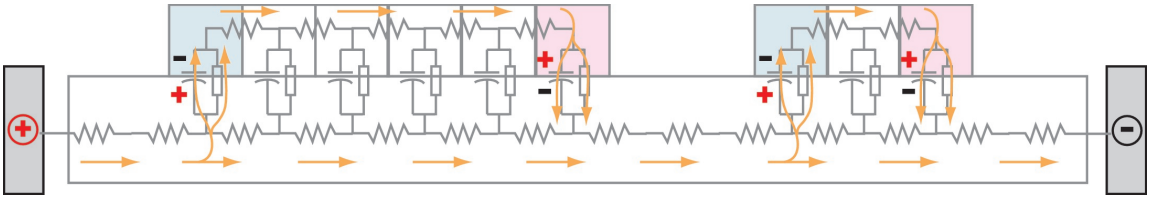

Figure 2: Depolarization and hyperpolarization of cardiac cells by an applied electric field. Reproduced from [3]

Because heart muscle cells are so interconnected, when one cell becomes excited, the action potential spreads. An action potential propagates as a positive deflection in the membrane

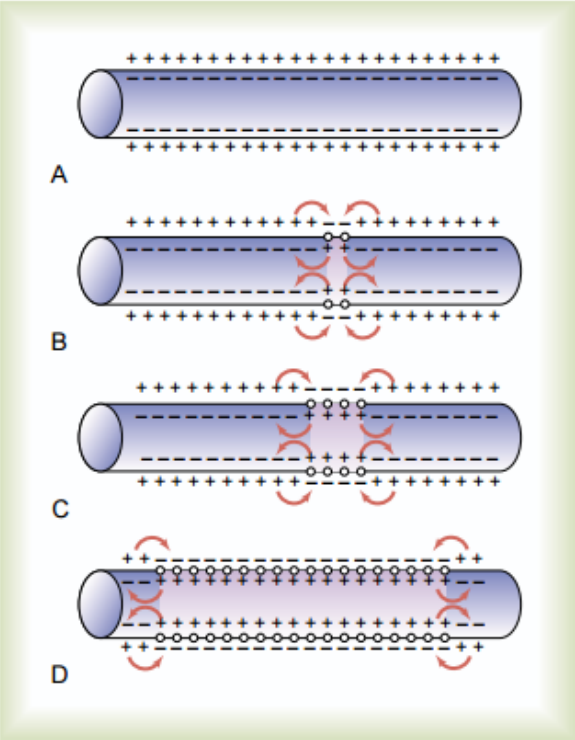

Figure 3: Action potential propagation over time [2]

potential, which is generated by diffusing positive ions flowing out ahead of the wave, through the gap junctions [2]. The membrane potential in adjacent cells is thereby increased over the action potential threshold, which in turn causes the sodium channels there to open. The propagation of action potential along a cable of cells can be seen in Figure 3. In the heart, contraction of muscles is caused by this propagation of action potentials [2]. The action potentials cause the release of calcium ions from the sarcoplasmic reticulum in the cell which diffuse and cause the chemical reaction that triggers muscle contraction.

The first to model the propagation of action potentials mathematically were Hodgkin and Huxley [4],[5]. They considered electrical propagation along a giant squid axon. As seen above, the principal ion currents in excitable tissue are sodium (Na^+) and potassium (K^+). Any other ions are assumed small and grouped together in a leakage current. (Note: calcium ions (Ca^{2+}) are also important in the heart, but are not required for the basic excitable and refractory properties, which are the two properties that are of importance to our study.) Hodgkin and Huxley assumed that action potentials do not affect the ion concentrations or equilibrium potentials. They developed a model for describing the propagation of action potential as a set of differential equations

dependent on four variables. This included the difference in potential from rest, potassium activation, sodium activation, and sodium inactivation. These variables can be categorized based on their behavior. The membrane potential and sodium activation variables change rapidly, while potassium activation and sodium inactivation change slowly. Because of this, FitzHugh and Nagumo [6],[7] later developed a simplified version of the Hodgkin-Huxley model, using only two variables representative of the fast and slow behavior [4].

In this study, we will use the Barkley model to represent action potential propagation in the heart. The Barkley model is similar to the FitzHugh-Nagumo model, containing only slight modifications that make certain properties easier to study. The Barkley model retains the properties most important for our study, namely the membrane potential and refractoriness of the medium, while its simplicity allowed us to modify the code easily and run it quickly on the computer.

I.2 What is Ventricular Fibrillation?

Fibrillation is the state of desynchronized action potential waves in the heart, which can occur in either the atria or ventricles. It can be caused by a mechanism called reentry [8]. Consider a ring of excitable homogeneous tissue to which an electrical stimulus is applied. Two action potentials form, which propagate both to the left (counterclockwise) and to the right (clockwise). As these waves continue around the ring, they run into each other, causing them both to stop. However, if a transient block, caused by inhomogeneities, is present in the ring, the action potential can only propagate in one direction. Since there isn't another wave to collide with, this wave continues around the entirety of the ring. If, by the time the wave returns to the block's position, the block is still present, the wave runs into it and stops. However, if the block is no longer there, the wave continues around the ring indefinitely, reactivating the initial stimulus spot repeatedly. This wave activity is known as reentry.

In this paper, we consider the presence of scroll waves as the primary cause of ventricular fibrillation. These waves are an idealization of reentry as described above. A scroll wave is a vortex-like wave of electrical activity in the heart. Unlike the electrical waves that are present in the heart during its normal functioning, scroll waves are self-sustaining and therefore persistent. Scroll waves also have a higher rotational frequency, meaning the heart beats faster in the presence of scroll waves. These properties prevent normal electric waves from forming. Since they also generally do not produce an efficient contraction of the heart, scroll waves severely compromise the pumping function of the heart.

Thus, after ventricular fibrillation is started, treatment needs to be applied quickly, generally within 3 minutes. Waiting longer than this can result in a lack of oxygenated blood to vital organs. Electrical defibrillation is the act of applying an electric shock to the heart to terminate ventricular or atrial fibrillation. The shock causes the depolarization of the myocardium (heart muscle), allowing the electrical current to return to its normal state. Direct or transventricular defibrillation uses electrodes applied directly to the ventricles [8]. Indirect or transthoracic defibrillation uses a shock applied to the outside of the body. Here, the entirety of the shock does not get applied to the ventricles and success in this method depends on the shock strength and electrical distribution across the body.

I.3 Previous Work

Many methods have been developed to terminate the scroll waves causing fibrillation. Currently, fibrillation is typically treated using cardioversion [3], the application of a large electric field to the heart. Cardioversion attempts to reset all the electrical activity in the heart, not just the scroll waves. Applying fields of this strength has its disadvantages, however, causing pain and trauma, damaging the myocardium, and reducing the battery life of implanted devices. To avoid these drawbacks, methods should either focus solely on the scroll waves or should have a smaller field strength. Another treatment currently used is antitachycardia pacing (ATP) [3]. In this treatment, a series of low-energy stimuli is delivered by a single electrode. This method is effective for treating tachycardia, which often occurs before fibrillation, but is much less effective against fibrillation itself.

A single scroll wave can be terminated with an electric pulse [9],[10] provided it is rotating around an anatomical feature (such as blood vessel, etc.) that is located close to a surface. However, this method is sensitive to the time at which the electric field pulse is applied. It is also not likely enough to completely terminate ventricular fibrillation since there is often more than one wave present. These waves have unknown location and phases. Hornung et al. [9] demonstrated that a series of electric field pulses in a technique called "phase scanning" can be used to deal with the problem of unknown wave phase leading to a higher, but still not perfect, success rate.

Considerable experimental progress in this area of low-energy defibrillation has been made by [3],[11], [12], in which multiple, low-energy field pulses, all pointing in the same direction, are applied. The method is thought to work by recruiting sites which act as "virtual electrodes". These electrodes appear around electrically heterogeneous features in the heart such as blood vessels

or in areas with an abrupt change in fiber direction. As electric stimuli are applied to the heart, these virtual electrodes can become depolarized and launch waves. At lower field strengths, only a few sites might activate, but as the field increases, more sites are recruited. This means that at certain field strengths, most of the tissue is depolarized and covered with a wave, leaving no room for the scroll waves. The hope is that this method, sometimes called far-field antifibrillation pacing (FF-AFP) [3], will be an improvement over standard cardioversion in that it requires much lower field strengths for successful defibrillation. Because this method utilizes low electric field strengths, it does not have the same disadvantages as cardioverson. That is, it does not result in pain, damaged heart cells, or reduced battery life of implanted devices.

In Ambrosi et al. [13], a series of low-energy shocks were able to terminate both atrial flutter and fibrillation in rabbit hearts. These shocks were applied rapidly, within one or two rotational periods. Ambrosi et al. found that the success of this method when terminating atrial fibrillation depended on the recruitment of sources as virtual electrodes as just described. They found that this method worked much better than both ATP and a single electric shock.

In Li et al. [12], the researchers applied the series of low-energy pulses in an attempt to stop ventricular tachycardia (VT) in an experiment done using rabbit hearts. Here, they found that ATP was not enough to terminate VT. Two types of shocks were applied in these experiments: monophasic (standard shock) and biphasic (shocks which change in polarity). The success of a single shock in both cases was dependent on the wave's phase. In cases when the shock was applied at the "wrong" time, a higher strength field was required for successful defibrillation. In this case, the hyperpolarization in the system caused a more rapid propagation, filling in the excitable gap with the wave. Since results of one shock were time-dependent, Li et al. then decided to apply five pulses within the span of one rotational period of the wave. This method was not dependent on the time of application. The later shocks prolonged the refractory period of the area excited by the initial shock. Since the area remained refractory for longer, the scroll wave was terminated as it attempted to rotate into that area. Li et al. also found that the monophasic shocks produced better results than the biphasic since the reverse in polarity in the latter resulted in some cancellation of the effects of the field.

Other work using low-energy field pulses has been done by Ji et al [14]. Their method, called LEAP (low-energy anti-fibrillation pacing), applied at least five low-energy electric pulses in both experiments, using canine hearts, and in simulation, using 2-dimensional tissue. In this method, the pulses entrained portions of the tissue to assist in the defibrillation process. More tissue became entrained as more pulses were applied. These regions were consequently synchronized, meaning

they had the same rotational phase. Once the majority of the tissue has been synchronized, it became easier to terminate all waves.

Computer simulation has proven to be a useful and flexible tool in the study of the defibrillation process. Use of computer models allows the researcher to either include or, perhaps as importantly, exclude anatomical features and/or dynamics. Being able to choose what is included in a model helps to uncover the mechanisms involved in the defibrillation process. Models for the ion channels involved in wave propagation then may be as detailed as modern, multivariable models ([15],[16],[17],[18],[19],[20]) or as simple as the FitzHugh-Nagumo ([6],[7]) or Barkley ([21],[22]) two-variable models. System geometries in these models vary from anatomically realistic models of the heart to 2- or 3-dimensional rectangular boxes ([9],[14],[23]) or one-dimensional rings ([24],[25]).

For example, Trayanova et al. [26] developed detailed models of the heart to understand how electric fields produce depolarization and hyperpolarization in the heart. When considering a spherical system [27], they found a cosine dependence of the depolarization and hyperpolarization on the system after the application of an electric field. This dependence is similar to what is seen in our hemispherical shell system (see below). Their bidomain model (describing both intra- and extracellular regions) utilized complex models to define details in the heart, such as membrane kinetics and ion channels. The application of a single electric shock in this model yielded similar results as seen in Ripplinger et al.'s [10] and Li's [12] work above. Specifically, they found that precise timing was needed in order to have successful defibrillation. They also found that deexcitation (or repolarization) created excitable gaps in the system. An increased shock strength could overcome these gaps, however, since the increased area which was being repolarized allowed the wave to propagate quickly, filling in the gaps.

On the other hand, Roth et al. [28] used the bidomain model in simplified geometry (2-dimensional box) and local dynamics (i.e., ion channel dynamics). They studied the effects of anisotropy (difference in the conductivities measured parallel and perpendicular to the fibers in the heart) on depolarization and hyperpolarization patterns around an electrode. Roth et al. found that different changes in fiber direction affected the way in which their system was depolarized and hyperpolarized.

Bragard et al. [24] and Otani [25] both used ring geometry. Bragard et al. [24] used the Beeler-Reuter equations [29] to describe the cells in their system. Three different types of shocks were applied to this system in an attempt to terminate the wave rotated along the ring. These included

monophasic and two types of biphasic shocks. In a biphasic shock, the polarity is switched during the shock application. Both a biphasic shock that had equal parts with both polarities and one that had uneven parts (more positive than negative) were tested. Bragard et al. found that the uneven biphasic shock was most successful and required less energy than the monophasic. Otani [25] used a simple model to describe the system called the coupled maps model. This model utilized virtual electrodes (like in [3] and [14]) to assist in termination. Otani applied two or three low-energy pulses to the ring in order to terminate the rotating wave present. The time between these pulses was varied and gaps a little longer than the wave's rotational period worked the best.

For the current study on new, low-energy defibrillation methods, we find it expedient to use simplified geometries and ion channel dynamics. These models are computationally fast to run and easy to analyze. Perhaps most importantly, simplified models allow us to focus on specific properties in the heart and determine their role in scroll wave termination. Previous studies related to our work also use simplified models. Biktashev [30] demonstrated that a scroll wave can be terminated by a plane wave that propagates parallel to the filament (i.e., the line or curve around which a scroll wave rotates). Zemlin et al. considered this method of terminating a single scroll wave in a 3D rectangular system in additional detail [23]. A monodomain FitzHugh-Nagumo model was solved using explicit Euler method with Neumann boundary conditions. An electric field shock was applied to the rectangular system, creating a thin slab of depolarization on the surface. While this surface depolarization was not enough to immediately terminate a scroll wave, it was enough to destabilize it. Once the wave was destabilized, defibrillation became successful as a result of the filament becoming C-shaped (attached to adjacent surfaces). This method can fail when the timing is not right, which depends on the wave's orientation, or when the filament created is I-shaped (attached to opposite surfaces). In this scheme, filaments tend to contract, meaning that an C-shaped filament contracts until it eventually disappears, whereas an I-shaped filament only contracts until it is straight. The shape of the created filament is dependent on the wave's orientation at the time of the shock. Because of this, Zemlin et al. believe that the filament structure can help predict the success of their method. The time it takes for the method to be successful depends on the size of medium and the position of the filament. That is, a small size or filament close to the boundary yields a shorter delay in success.

I.4 Our Defibrillation Strategy

The model presented here utilizes methods of applying a series of low-energy electric fields in an attempt to defibrillate multiple scroll waves. This method does not require knowledge of scroll wave number, location, or phase. As seen in [23], [30] and [31], an electric field applied parallel to the filament around which a scroll wave is rotating is capable of terminating the wave, generally independent of its phase. This occurs because the back surface of the system is depolarized, pushing the filament attached to it onto an adjacent wall. This newly formed C-shaped filament then contracts and disappears. We use this to inform our new defibrillation strategy.

Our strategy utilizes a set of electric field pulses which modify all scroll waves in the system in a way which they will contract and disappear. Our set of electric field pulses, applied in different directions, depolarizes the entire outside surface of our system. All filaments, which are connected to that surface, are then necessarily detached from that surface. The newly formed filaments will then tend to be either C-shaped (as in [23],[31]) or U-shaped (connected to same surface). Scroll waves which have filaments with these shapes then shrink and disappear. If all of the filaments in our system have been affected in this way, we have termination of all waves and, in turn, successful defibrillation. There are some instances in which this method fails to work, which will be discussed later.

In the past, many have only considered a single scroll wave in a rectangular system. Instead, we present between one and four scroll waves in a hemispherical shell system. The advantage of this method is that, unlike in cases mentioned above, we are not required to know the location of the scroll waves. We test our method on various wave orientations to ensure that it is also independent of that.

II. Methods and Equations

II.1 Deriving Equations

We begin by deriving equations representative of the behavior of heart cells. Here, heart cells can be represented by circuits, as shown in Figure 4. Gap junctions between cells are represented by resistors. Cells communicate with the extracellular space via either the cell membrane, shown as a capacitor, or ion channels, shown as boxes. The extracellular space is also represented with a series of resistors. The circuits are stimulated by electrodes inserted both inside and outside the cells. In our case, the stimulus comes from outside the extracellular space, as in Figure 2.

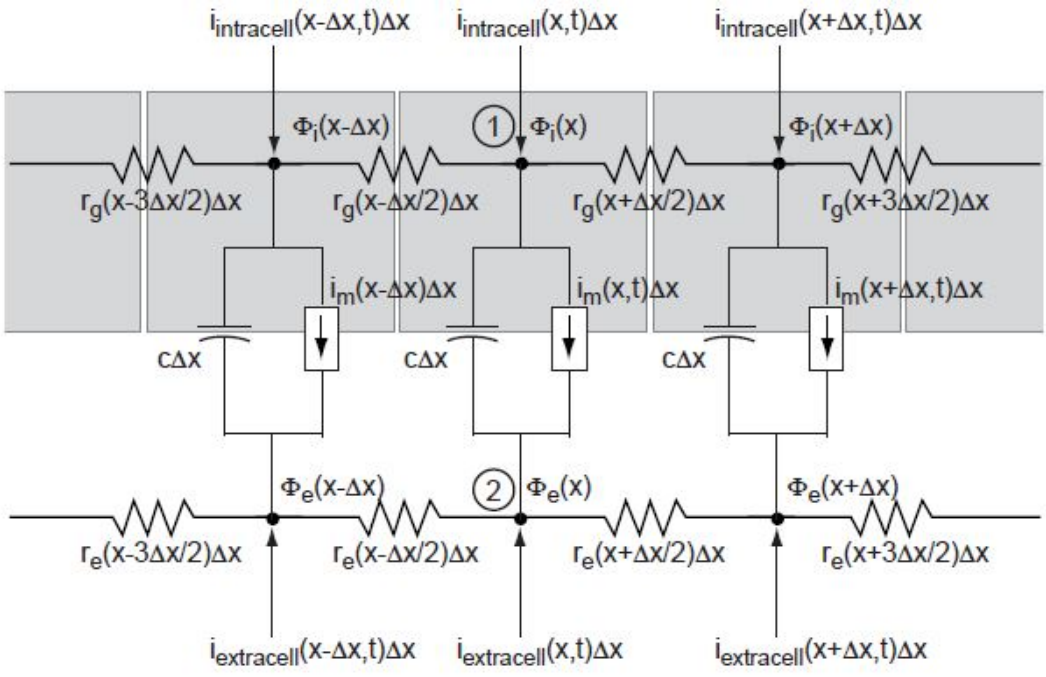

Figure 4: Complete circuit representation of heart cells

If we let the center of a given cell be represented by x and the length of a cell be Δx, then a coordinate system can be created for all cells in the x direction. The potential of each node, both intracellular and extracellular, is denoted as $\Phi_i(x)$ and $\Phi_e(x)$. Resistance in a gap junction and in the extracellular space is represented by $r_i\Delta x$ and $r_e\Delta x$ respectively. Similarly, membrane capacitance is represented by $c\Delta x$, and current flowing through an ion channel by $i_m\Delta x$. Since we have a coordinate system for every node, all of the above values can be written using this coordinate system.

Next, this model is used to create our equations. Kirchhoff's current law, which says that the total current flowing into and out of a node must sum to zero, applied to node 1 in the figure informs our first equation when we let $\Delta x \to 0$:

$$c\frac{\partial u}{\partial t}(x,t) + i_m(x,t) - \frac{1}{r_i}\frac{\partial^2 \Phi_i}{\partial x^2}(x,t) - i_{intracell}(x,t) = 0 \tag{II.1}$$

Note that the membrane potential u is equivalent to $\Phi_i(x) - \Phi_e(x)$. Making the substitutions $\Phi_i = u + \Phi_e$ and $D_g = \frac{1}{r_i c}$ produces the first of the cable equations:

$$\frac{\partial u}{\partial t} = -\frac{i_m}{c} + D_g\frac{\partial^2 u}{\partial x^2} + D_g\frac{\partial^2 \Phi_e}{\partial x^2} + \frac{i_{intracell}}{c} \tag{II.2}$$

Similarly, this law can be applied to node 2 by flipping the figure upside down and switching the intra- and extracellular components, yielding,

$$c\frac{\partial(-u)}{\partial t}(x,t) - i_m(x,t) - \frac{1}{r_e}\frac{\partial^2 \Phi_e}{\partial x^2}(x,t) - i_{extracell}(x,t) = 0 \tag{II.3}$$

Combining this equation with the first and substituting $D_e = 1/(r_e c)$ gives us the second cable equation:

$$(D_e + D_g)\frac{\partial^2 \Phi_e}{\partial x^2} = -D_g\frac{\partial^2 u}{\partial x^2} - \frac{i_{intracell}}{c} - \frac{i_{extracell}}{c} \tag{II.4}$$

For the purpose of our research, we use the monodomain Barkley equations ([21],[22]), a version of the cable equations. In the monodomain equations, we assume the extracellular potentials $\Phi_e(x)$ are zero. Equation (II.2) then no longer depends on Eq. (II.4), so we can ignore the latter equation. The Barkley model employs a relatively simple model for the ion channel currents. Specifically, $f(u,v)$, which depends on the membrane potential, u, and a variable measuring refractoriness, v, replaces the ion channel term. Therefore, Eq. (II.2) becomes,

$$\frac{\partial u}{\partial t} = D\frac{\partial^2 u}{\partial x^2} + f(u,v) + \frac{i_{intracell}}{c} \text{ where } f(u,v) = \epsilon^{-1}u(1-u)\left(u - \frac{v+b}{a}\right) \tag{II.5}$$

The Barkley model defines the evolution of v by,

$$\frac{\partial v}{\partial t} = u - v \tag{II.6}$$

Thus, Eqs. (II.5) and (II.6) are our model equations, where D, ϵ, a and b are parameters.

Studying Equation (II.5) provides insight about the behavior of action potential wavefronts in this system. Within the wavefront, the slowly-varying variable v is approximately constant. Thus, Eq. (II.5) may be written approximately as,

$$\frac{\partial u}{\partial t} = D\frac{\partial^2 u}{\partial t^2} + f(u) \tag{II.7}$$

We further assume that the wave velocity c and the wave shape are constant. Based on these assumptions, we can rewrite $u(x,t)$ as $U(\xi)$ where $\xi = x - ct$ describes the wave's current position relative to the position of the wave at time t. We plug this into Equation (II.7) and simplify.

$$\frac{\partial}{\partial t}U(\xi) = D\frac{\partial^2}{\partial x^2}U(\xi) + f(U(\xi))$$

$$-cU'(\xi) = DU''(\xi) + f(U(\xi))$$

Suppose that $dF/dU = f(U)$. We also multiply both sides by $U'(\xi)$ to get

$$-c(U'(\xi))^2 = DU'(\xi)U''(\xi) + \frac{dF}{dU}U'(\xi)$$

$$-c(U'(\xi))^2 = D\frac{d}{d\xi}\left[\frac{1}{2}(U'(\xi))^2\right] + \frac{dF(U(\xi))}{d\xi}$$

$$-c(U'(\xi))^2 = \frac{d}{d\xi}\left[\frac{1}{2}(U'(\xi))^2 + F(U(\xi))\right]$$

We now take the integral of both sides from $-\infty$ to ∞:

$$\int_{-\infty}^{\infty} -c(U'(\xi))^2 d\xi = \int_{-\infty}^{\infty} \frac{d}{d\xi}\left[\frac{1}{2}(U'(\xi))^2 + F(U(\xi))\right] d\xi$$

$$-c\int_{-\infty}^{\infty} (U'(\xi))^2 d\xi = \left[\frac{1}{2}(U'(\xi))^2 + F(U(\xi))\right]_{-\infty}^{\infty}$$

If we focus only on the wavefront of an action potential, which is very sharp, the slope of the wave should go to 0 as $\xi \to \pm\infty$, as seen in Figure 5. So, $U'(\xi)$ evaluated at $\pm\infty$ are both zero. This leaves $F(U(\infty)) - F(U(-\infty))$ on the right hand side. Recall that $dF/dU = f(U)$. This means that we have

$$-c\int_{-\infty}^{\infty} (U'(\xi))^2 d\xi = \int_{U(-\infty)}^{U(\infty)} f(U)dU$$

The bounds on u provides values for the bounds of the right side integral.

$$-c\int_{-\infty}^{\infty} (U'(\xi))^2 d\xi = \int_{0}^{1} f(U)dU$$

We are concerned with the case for which the wave stops propagating, in other words, we want to determine the value of refractoriness that satisfies the above equation when $c = 0$. Therefore we can solve

$$\int_0^1 f(U)dU = 0$$

Here, $f(u) = \epsilon^{-1}u(1-u)\left(u - \frac{v+b}{a}\right)$.

$$\epsilon^{-1}\int_0^1 \left(u(1-u)\left(u - \frac{v+b}{a}\right)\right) du$$

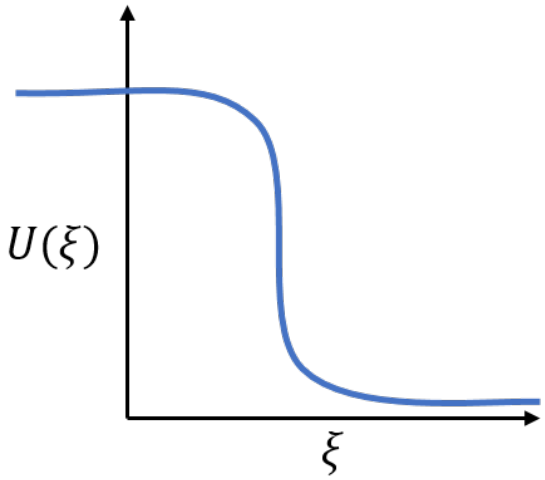

Figure 5: Wavefront shape assumed for the function $U(\xi)$ in the evaluation of Eq. II.7

$$
\begin{aligned}
&= \epsilon^{-1} \int_0^1 \left(u^2 - \frac{v+b}{a} u - u^3 - \frac{v+b}{a} u^2 \right) du \\
&= \epsilon^{-1} \left[\frac{u^3}{3} - \frac{v+b}{2a} u^2 - \frac{u^4}{4} + \frac{v+b}{3a} u^3 \right]_0^1 \\
&\\
&-\epsilon^{-1} \left(-\frac{1}{12} + \frac{v+b}{6a} \right) = 0 \\
&v = \frac{a}{2} - b
\end{aligned}
\tag{II.8}
$$

Therefore, we expect $v = a/2 - b$ to be the refractory threshold that stops a wave from propagating.

II.2 Computer Simulation

In our computer simulations, we solved the Barkley equations (II.5) and (II.6) using a simple forward Euler method. We chose parameters $a = 0.8$, $b = 0.05$, $D = 1$ and $\epsilon = 0.02$. These parameters are in the collapsing scroll ring regime as discussed in [32]. The system has a grid spacing of $1/6$ and a time step of 1.6×10^{-3}. These values are dimensionless parameters. Barkley units in this system correspond approximately to the real values 1mm and 20ms. That is, 1 timestep is equivalent to 0.032ms and 1 grid space is equivalent to $(1/6)$mm.

When no electric fields were being applied, we used no-flow boundary conditions, which is consistent with zero current flow into the system from the exterior region. A convenient way

to think about the application of an electric field, when it is being applied, is to consider it as a change in the boundary conditions to represent the current injected into the system caused by the electric field. Consequently, the effects of an electric field can be represented as the injection of intracellular current to cells residing on the surface of the system. Zemlin et al. [23] used a similar strategy, modeling an electric field pulse by applying the following current to the cells adjacent to the system surface:

$$I_{shock}(x) = I_0 \frac{\sinh(x - x_m)/\lambda}{\sinh x_m/\lambda}$$

where x is position along cross section of the wall with x_m being the midpoint, λ is characteristic attenuation length, and I_0 is the shock current amplitude. They used $x_m = 4.25$mm, $\lambda = 500\mu$m, $I_0 = 3\mu\text{A/cm}^2$ for a duration of 9.6ms, relative to their system.

In our study, we used a method created by Pumir [33], which only injects current into cells right on the surface according to the formula $I_{intracell} = (1/r_i)\hat{\mathbf{n}} \cdot \mathbf{E}_0$, where r_i is the intracellular resistance per unit length defined earlier, $\mathbf{E}_0$ is the applied electric field and $\hat{\mathbf{n}}$ is the outward-pointing unit vector pointing normal to the system surface.

While we see similar results as Zemlin, there are some notable differences. We believe Pumir's method is correct, because the sinh behavior imposed by Zemlin naturally occurs after an electric field as defined by Pumir is applied. The sinh behavior can be obtained by solving II.4 for the extracellular potential term and plugging into II.2:

$$\frac{\partial u}{\partial t} = -\frac{i_m}{c} + D_g \frac{\partial^2 u}{\partial x^2} - \frac{D_g^2}{D_e + D_g} \frac{\partial^2 u}{\partial x^2}$$

To mimic calculations done by Zemlin, we consider a steady state solution and combine the membrane potential terms:

$$0 = -\frac{i_m}{c} + D\frac{\partial^2 u}{\partial x^2} \text{ where } D = \frac{D_g D_e}{D_e + D_g}$$

If we use a linear approximation for the ion current, $i_m = g_m u$, where g_m is the membrane conductance per unit length, this equation has an exponential solution which we assume has the form $u = u_0 e^{kx}$. Plugging this solution into the equation above yields:

$$\frac{g_m}{c} u_0 e^{kx} = Dk^2 u_0 e^{kx}$$

Simplifying this we get $k = \pm\sqrt{g_m/(cD)}$. This becomes $k = \pm\sqrt{g_m r}$ since $D = 1/(rc)$. Note that $\lambda = 1/k$ is the characteristic space length. Therefore, the solution to the cable equations is

$$u(x) = u_1 e^{x/\lambda} + u_2 e^{-x/\lambda}$$

For $u_0 = u_1 = -u_2$ this is equivalent to $2u_0 \sinh(x/\lambda)$. The value of u_0 here is determined by the boundary conditions implemented with Pumir's formula.

Four types of simulation systems were used: (1) two-dimensional-like rectangular systems, (2) three-dimensional boxes, (3) three-dimensional cylindrical systems and (4) three-dimensional hemispherical shells. Two-dimensional rectangular systems were used to find the basic propagation properties of plane and curved action potential waves. The 3D boxes and cylinders were used to study some key scroll wave termination properties. The hemispherical shell was used to test our new defibrillation protocols.

Scroll waves in this system were created using cross-field stimulation. A plane wave was started at one side of the system. As the trailing edge of this wave passed through the center of the system, another wave was initialized perpendicular to the first wave. The scroll wave started to rotate around the intersection of these waves. Applying the second wave at different times or locations allowed us to form multiple scroll waves. The scroll waves formed in this system were allowed to rotate three times in order to ensure they settled down before any fields were applied.

We first looked at a single scroll wave in a box-shaped and cylindrical system. These were used to test our theories about the mechanisms causing defibrillation failure. An electric field with varying strengths was applied to the back wall of the surface, parallel to the wave's filament.

Next, we considered a hemispherical shell system. This more closely resembles the ventricles of the heart and limits the number of surfaces that the filament can attach to. The shell was defined within a rectangular 3D box as the volume between two radii, inner 19.99 grid points and the outer 39.99 grid points. The radii were measured from a point at the center of the top surface of the box. Functionally, the hemispherical shell was defined by eliminating all gap junctions, represented by segments between points, in the grid for which at least one end lay outside the volume defined by the two radii.

When applying electric fields, we depolarized one surface and hyperpolarized the opposite surface using Pumir's formula (see above). The shell is comprised of many flat surfaces as shown in Figure 6. When applying an electric field in the negative x direction (i.e., pointing to the left), we want to depolarize (blue) all surfaces facing to the left and hyperpolarize (red) all surfaces facing in the opposite direction. We run through all potential gap junctions in the negative x direction to determine which faces get depolarized and hyperpolarized. The code identifies surfaces which get hyperpolarized as those which transition from no gap junction (outside system) to a gap junction (inside system). The opposite is true for surfaces that get depolarized. Specifically, the code runs

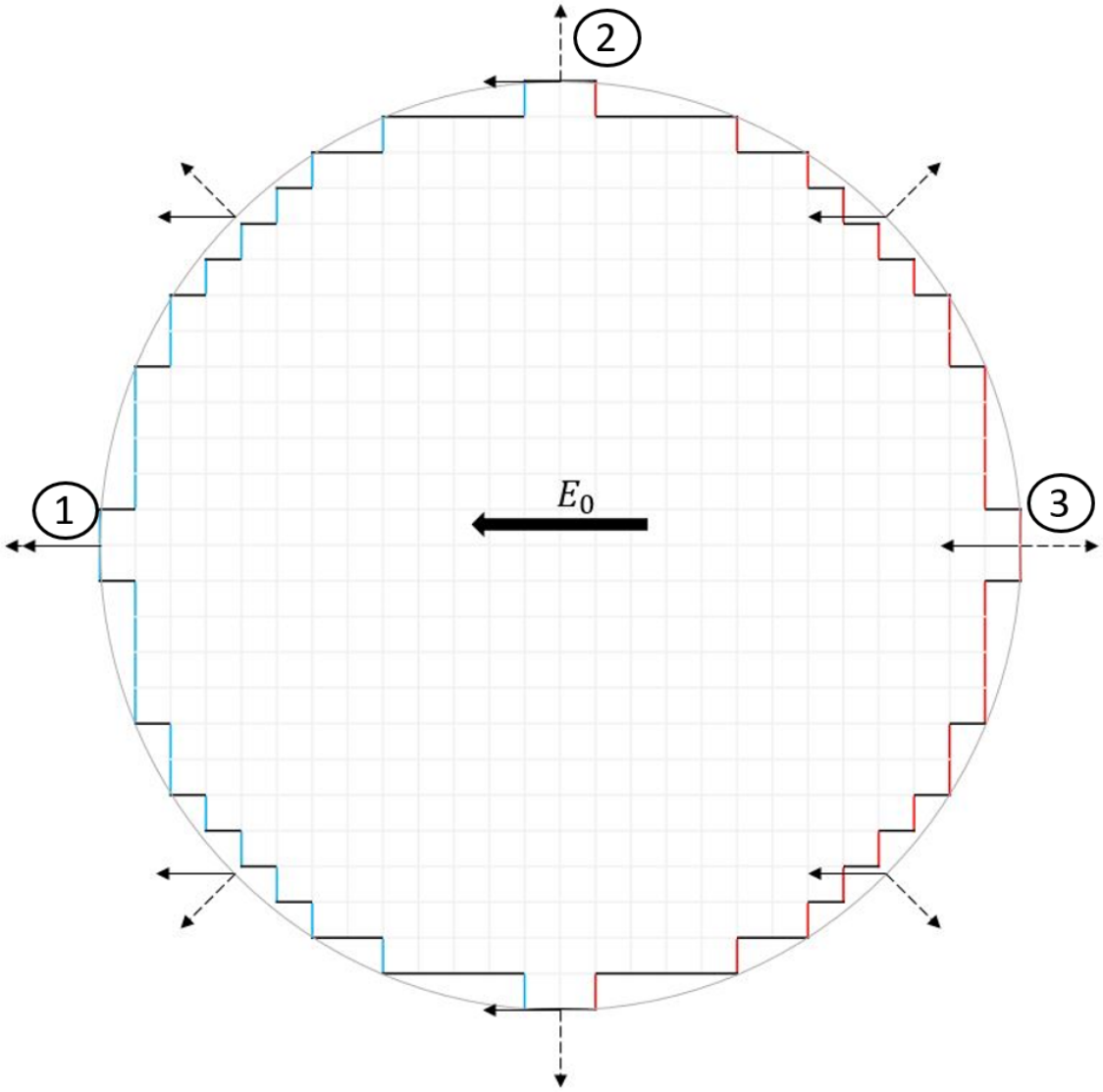

Figure 6: Scheme for depolarization (blue) and hyperpolarization (red) in top of hemispherical shell. Electric field is applied right to left. Dashed arrows represent normal vectors to circle and solid arrows represent electric field direction

through all points in the system going in the negative x direction and checks whether they are within the set of radii. If a point is inside the boundary but the previous one was not, the code identifies that point as one which gets hyperpolarized. The code then runs the above procedure in the opposite direction to determine points which get depolarized.

As previously mentioned, we inject current in this system according to Pumir's formula $I_{intracell} = (1/r_i)\hat{\mathbf{n}} \cdot \mathbf{E}_0$. In Figure 6, a top view of the hemispherical shell is shown (aside from the inner surface). The effect of an applied electric field is to depolarize surfaces facing towards the negative electrode, and hyperpolarize surfaces facing in the opposite direction. Figure 6 shows how this applies to our computational model. All blue line segments (representing square surfaces in 3D) face to the left, towards the negative electrode; thus we inject current into these surfaces, depolarizing them. Analogously we draw current out of surfaces represented by the red line segments.

We observe that this scheme is consistent with Pumir's formula, as seen in Figure 6. We see that at point 1, there are many depolarized (blue) line segments close together per unit distance. As we move from point 1 to 2, these faces become fewer and farther between. This implies that less current should be applied in areas where there are less faces. The number of blue segments around the circumference of the shell goes as $cos\theta$ around the left half of the shell, where θ is the angle between the normal vector to the curve and the electric field vector. As we look at point 1 in the figure, both vectors point in the same direction ($\theta = 0$). This means that cosine at the point is 1 and the entirety of the electric field is injected. As we move from point 1 to 2, the angle increases until it reaches 90°. The current injected during this time decreases until it reaches the top where cosine is 0. Similarly, the number of red line segments goes as $-\cos\theta$ on the right half.

The computer simulation plots waves according to the membrane potential value at all points in the system. A point is said to be in the action potential if its potential is above a value of b/a, 0.0625 for our model. Note that b/a is the firing threshold of cells when refractoriness is zero (see equation II.5). Points inside the action potential are plotted as an opaque region. Points with potential of b/a are identified as being either on the wavefront or waveback. This is determined by whether the membrane potential time derivative, $\partial u/\partial t$, is positive (wavefront) or negative (waveback). Those surfaces are colored bright red and bright blue, respectively, in our plots. Regions for which the potential is less than b/a are shown as being empty since they lie outside of the action potential. The cross-section of the wave along the surfaces of the system is shown as a range of muted colors representing different membrane potential values inside the action potential. Once all points in the system have membrane potential less than 0.001, defibrillation is

deemed successful and the code stops.

The filament around which a scroll wave rotates is identified as all points along the surface comprised of the wavefront and waveback for which the change in membrane potential is zero. This means that on one side of the point, the potential is increasing (wavefront) and on the other it is decreasing (waveback). Points along the filament are represented in green. Points within one grid space of the top surface are colored pink, within two grid spaces of the outer surface are colored black, and within two grid spaces of the inner surface are colored blue. In some cases, the filament plotting algorithm can falsely identify filaments or incorrectly classify the color of the filament when the filament gets very close to a surface (within the ranges stated above). Analysis of the system is needed to determine when this happens.

In this paper, we refer to different shapes of the filament with regards to the surfaces it connects to: I-shaped connect opposite surfaces, C-shaped connect adjacent surfaces, and U-shaped connect to the same surface, as shown in Figure 7.

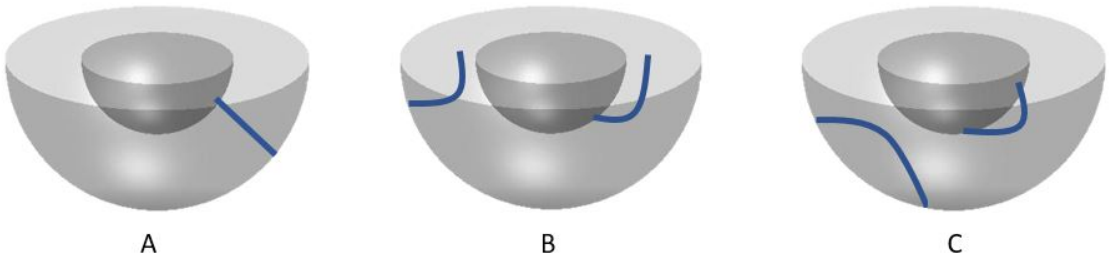

Figure 7: Filament orientations: (A) I-shaped, (B) C-shaped, and (C) U-shaped

III. Building Concepts

III.1 Threshold and Effect of Curvature

To better obtain knowledge of the propagation threshold of a scroll wave, we first launched a plane wave in a thin rectangular box, which we effectively ran as a 2D simulation. The refractoriness, v, of the box was set to a value and this value remained constant over time by setting $\partial v/\partial t = 0$. The propagation threshold is defined as the refractory value v which prevents a wave from propagating. That is, v values below the threshold allow a wave to propagate. When setting v equal to the expected threshold, $a/2 - b$ (from Eq. II.8), the plane wave did not propagate. However, decreasing the refractoriness by just 0.01 allowed the wave to propagate. We see that the closer the potential, u, in the system was to the propagation threshold, the slower the wave propagates. Note that these results are approximate as v generally depends on time.

Since we are modeling spiral waves and not plane waves, we next wanted to see how curvature affects a wave's ability to propagate. In theory, the threshold of propagation for a convex curved surface should be lower than that of a plane wave. This is because there is a source-sink imbalance. In a plane wave, cells on either side of the wave front match up exactly and the action potential can propagate nicely. In a convex curved surface, for example a circle, there are more cells in front of the wave front than inside it. This means that a smaller number of cells in the wave are supplying current to a larger number of cells ahead of the wave. This imbalance slows down the wave, sometimes resulting in wave termination if the imbalance (i.e. the wave curvature) is large enough.

To test this theory, we launched both a disk-shaped wave in the 2D rectangular system, and a spherical wave in the 3D box system. A variety of radii were tested and the curvature and propagation threshold in each case were recorded, shown in Figure 8. As expected, we found that as the curvature increased, the propagation threshold decreased. Again, the closer the refractoriness of the system was to the threshold, the slower the wave propagated. Figure 8 shows the largest value of v that allows propagation of waves of various wavefront curvatures in 2D (disk-shaped waves) and 3D (spherical waves). Curvature for the disk-shaped and spherical waves are defined as $1/r$ and $2/r$, respectively, where r is the radius of curvature of the wave. These definitions of curvature are based on the fraction of source cells to sink cells. The near overlap of the two curves in Figure 8 is consistent with the source-sink imbalance created by the curvature of the wave being responsible for the dependence of the critical value of v.

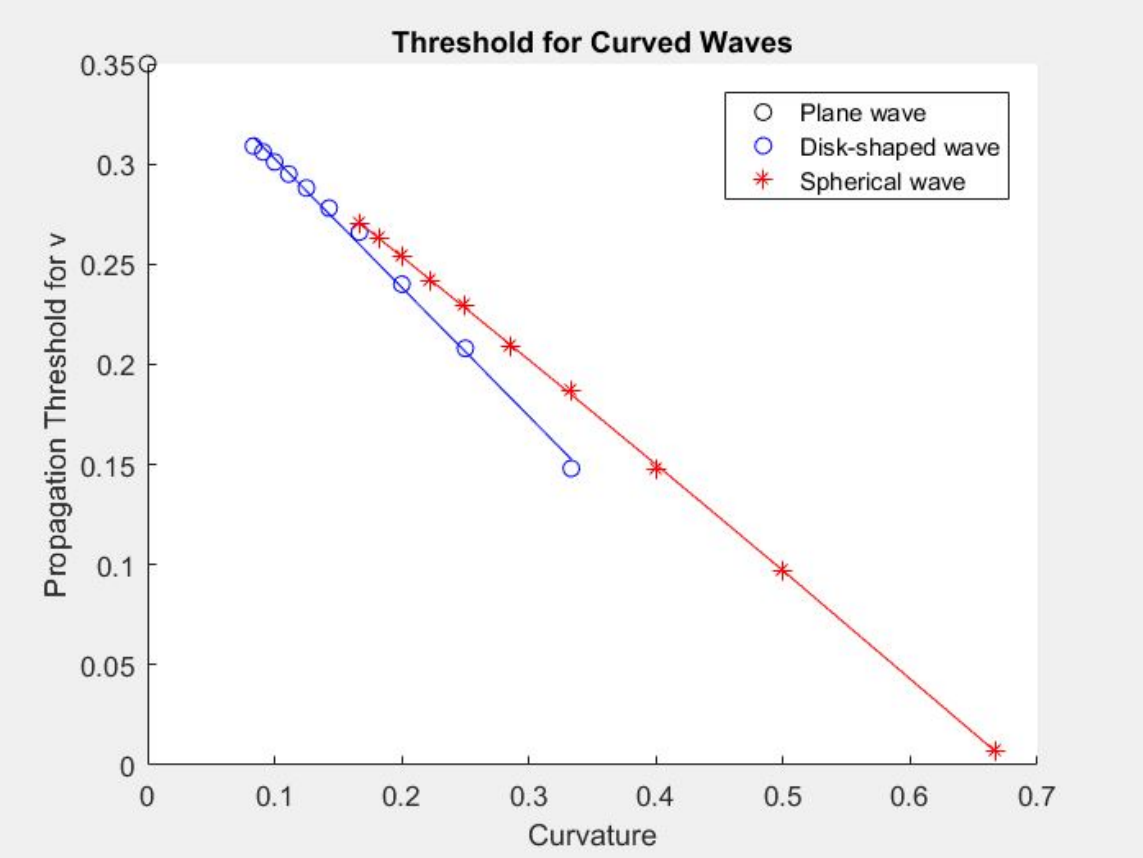

Figure 8: Maximum values of v for which wave propagation is possible vs. curvature of the wavefront, for disk-shaped waves (blue) and spherical waves (red). Lines of best fit are drawn.

III.2 3D Rectangular and Cylindrical Simulations

We next considered a single scroll wave in a rectangular box system, similar to that in [23]. Two plane electrodes were situated at the front and back of the box. This is similar to the point electrodes used for standard defibrillation except that it produces an electric field that is more spatially uniform in strength than is possible with point electrodes. Figure 9 shows an example of successful termination of a scroll wave in a 3D rectangular system using plane electrodes. In the simulation, an electric field with strength of 2.2V/cm was applied across the system, parallel to the I-shaped filament (white dashed line), causing the back wall to become depolarized. The initial filament became C-shaped, connecting to the front wall and the top of the box. The scroll wave continued to rotate around the now C-shaped filament shrinking until it disappeared.

We also created a cylindrical system using the same method of eliminating gap junctions as was used to create the hemispherical shell system. Electric fields with different strengths were applied to the system to determine the minimum strength for which termination was successful. The fields were applied at six different times, each one-fifth of the waves rotational period apart, to test whether success depended on the wave's phase. Here, the scroll wave was terminated for an electric field strength of 1.0753V/cm but failed to terminate for a strength of 0.9677V/cm for all six stimulus times. Figure 10 describes the possible outcomes after the application of a single electric field pulse. In the top row, a field strength of 0.9677V/cm was applied. After two rotations, the filament returned to I-shape and persisted. In the bottom row, a field strength of 1.0753V/cm was applied. Here, the filament remained C-shaped after two rotations. This filament continued to shrink until it disappeared.

One major way in which this method fails is by the reconnnection of the filament to opposite walls, that is, the C-shaped filament returns to an I-shape. This can occur when the filament moves too close to the wall. Figure 11 shows one wall in the rectangular system. The color gradient seen in the plots represents different values of v in the system, with blue being values close to zero and red close to one. The black line represents the threshold value of v and the red line outlines the wave. The intersection of these lines locates where the filament is attached to the wall. In the case when termination fails (left panel), we see the intersection move towards the edge. The wavefront was able to make it through the corridor between the filament and the right-hand wall but has a larger curvature than the corresponding wavefront in the panel on the right. As we have seen, an increase in the wavefront curvature makes it more difficult for the wave to propagate, which lowers the level of refractoriness v needed to stop the wave below its plane wave value of $a/2 - b$.

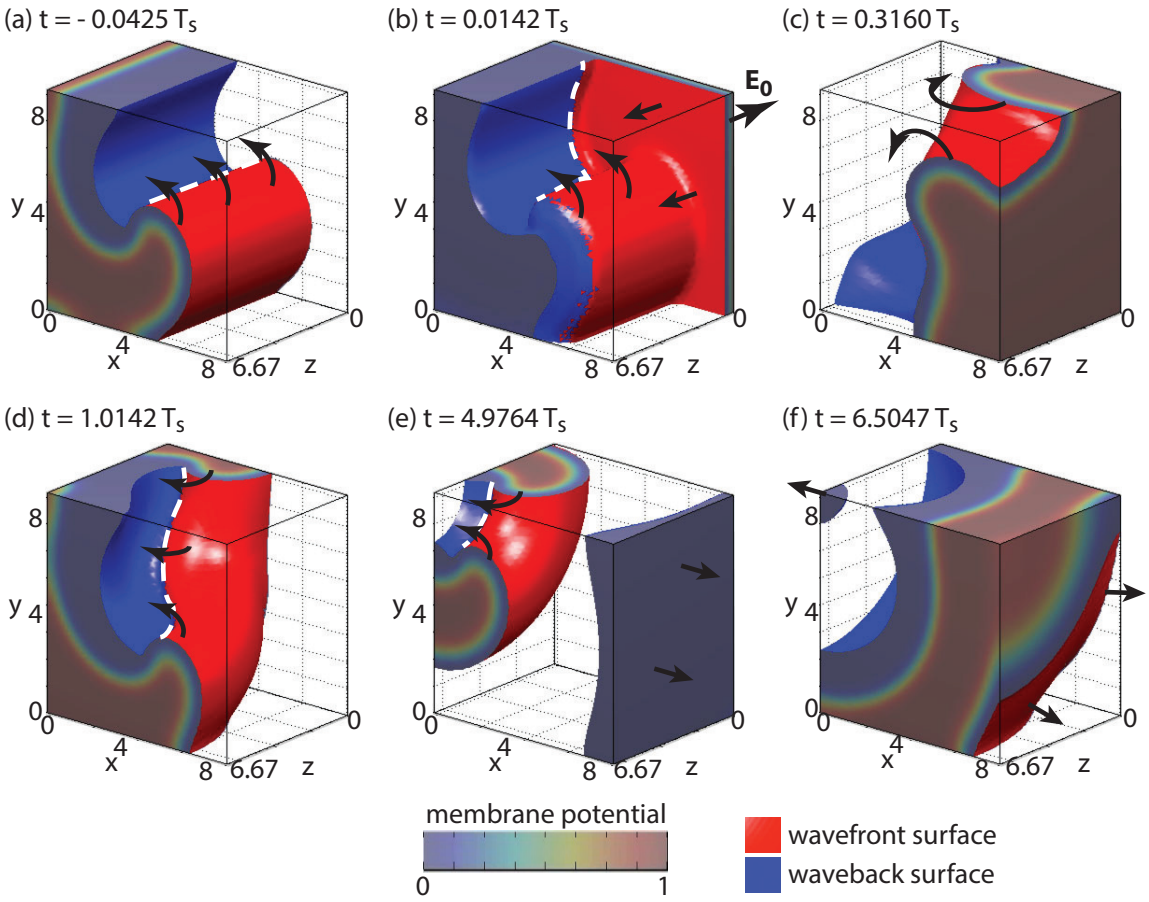

Figure 9: Successful termination of a scroll wave in 3D rectangular system. Electric field applied in the direction shown in panel (b) had strength 2.2V/cm. Axes are in terms of Barkley units and T_s is the scroll wave's rotational period. The wave's rotational direction is represented using the black arrows and the filament is shown as a dashed white line. The manner in which colors are used is describe in the Computer Simulation section. From [31].

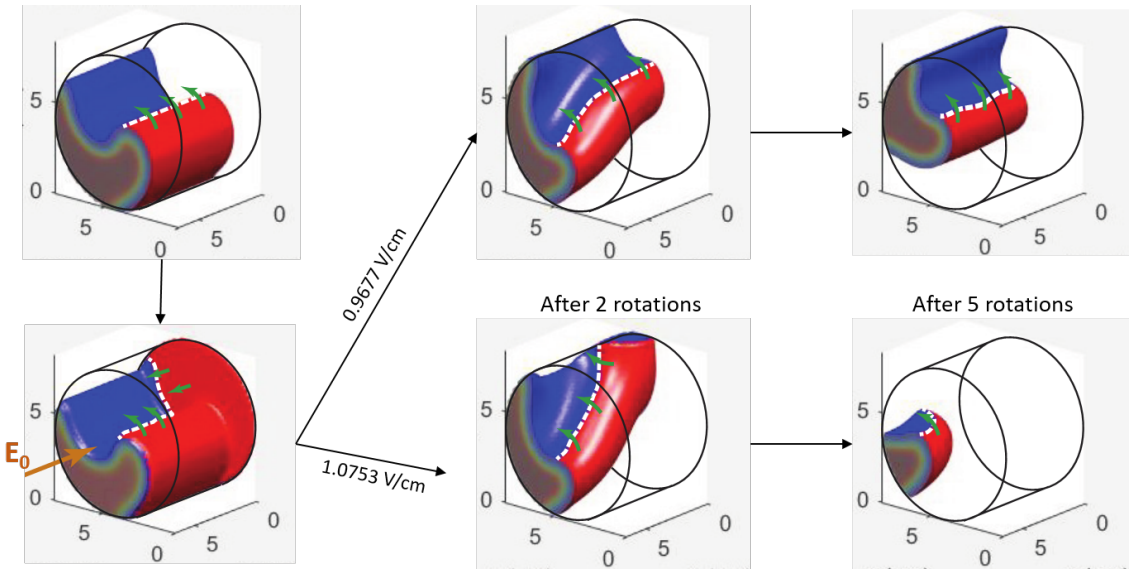

Figure 10: Single electric field pulse applied to cylindrical system (direction shown in bottom left plot). In the top row, a field strength of 0.9677V/cm was applied. The filament quickly reconnects to the back surface and continues to persist. In the bottom row, a filed strength of 1.0753V/cm was applied. Here, the filament remains C-shaped, shrinks, and disappears. All axes labels, colors, lines, and regions are defined in the same manner as in Figure 9.

This could cause the wavefront to become stuck (velocity becomes 0), unable to propagate forward. As the wave back continues, it forces the filament to move rightwards until it reaches the edge. Once this happens, the filament becomes connected to the adjacent wall and results in an I-shaped filament.

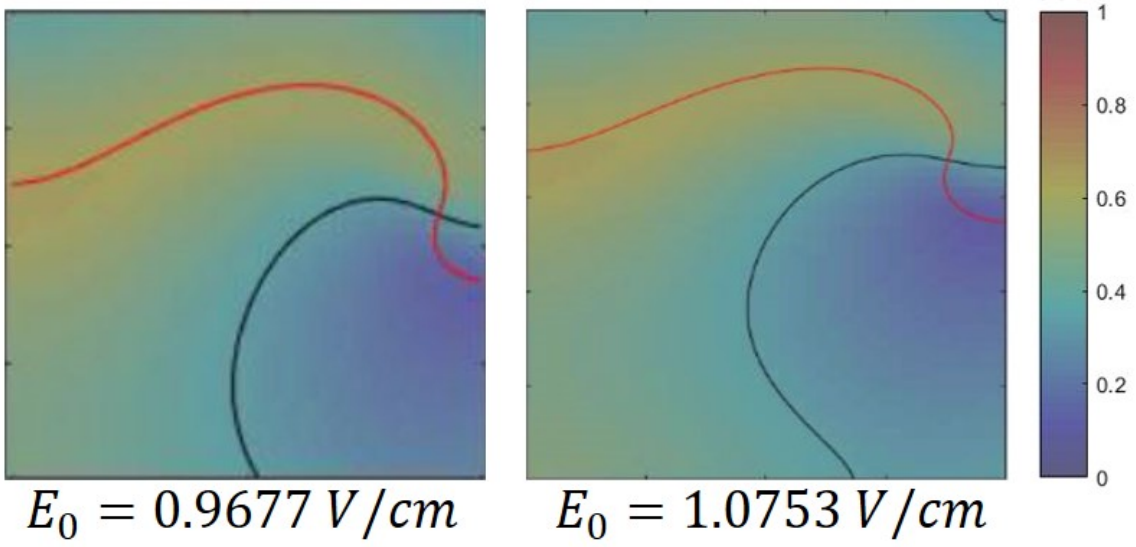

Figure 11: Curvature of wavefront (red) along side wall of 3D rectangular system in unsuccessful (left) and successful (right) scroll wave termination. Color gradient shown represents different values of v (shown in color bar to right). Black line represents the value of v which is the propagation threshold. The intersection of the red and black lines locates filament's attachment to wall. Stills taken 57ms after electric field application

IV. Proposed New Defibrillation Ideas in the Hemispherical System

We now present our proposed defibrillation schemes in a hemispherical shell system. We use this system because it more closely resembles the ventricles of the heart and limits the number of surfaces that the filament can attach to. Several new schemes for defibrillation are presented in this system. These include (1) a single electric field pulse, (2) two different series of five electric field pulses, and (3) a prolonged electric field pulse whose direction varies sinusoidally with time. Electric fields in the first two of these schemes are applied for 2.528ms and for 11.488ms in the last. The direction in which electric fields are applied vary between schemes. Each of the schemes listed above was chosen for its ability to depolarize the outside surface of the system.

Each scheme is tested for its ability to terminate one, two, three or four scroll waves. These waves are created in the system without detailed attention to their location, chiralities or distance from other scroll waves. Note that since these waves are created using cross-filed simulation, chiralities in the system tend to be balanced. We want our methods to be successful independent of a wave's location, orientation and phase. In each scheme, the application of electric fields is tested at six times that are one-fifth of the waves' rotational period apart. Electric field strengths tested typically range from 0.3077 to 2.4615V/cm but, in some cases, are increased until successful termination is achieved for all six timings of the electric field pulse(s). It is important to note here that the standard electric field strength used today is 5V/cm. Because of this, no fields used have strengths greater than this standard.

Success rates are calculated using results from 1.5 to 2.5V/cm and only include the first five stimulus times. This prevents double counting as the first and last times are typically the same (since the wave phases are the same). Two types of success rates are included, shown in Figure 12. Case success rates are calculated for each number of waves separately and depend on the number of successful simulations over the total number of simulations. Overall success rates are calculated over all number of waves for each scheme. This rate depends on the number of columns in which there is successful termination over the total number of columns.

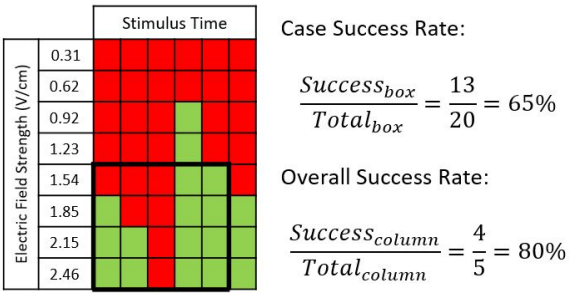

Figure 12: Portion of results taken from Figure 16. Green represents successful termination and red represents failed termination. Success rates are taken from data included in outlined box. Case success rate depends on the fraction of boxes (simulations) that represent success and overall success rate depends on the fraction of columns (application times) showing successful termination.

IV.1 Results

IV.1.1 Single Electric Field

The first defibrillation scheme tested was a single electric field. A single stimulus was applied in the y-direction. This was done as a point of comparison to the schemes presented below. This single stimulus is equivalent to the standard rectangular box model discussed in the "Building Concepts" section. We see that in the presence of one, two, three, and four waves, this method had case success rates of 0%, 40%, 15%, and 0% respectively (top row of Figure 16). The overall success rate for this scheme was 15%. Because a single field applied in this direction only depolarized half of the system, it is understandable that success rates here are rather low.

Next, a single electric field was applied in the z-direction (not shown in figure). This field depolarized most of the outside surface and was the first attempt at defibrillation. While most of the outside surface was depolarized, the area along the top rim was not. This follows a similar argument as is seen in Figure 6. That is, there are few surfaces near the top of the system at which current is being injected. Because there are so few places where current is injected at the top of the system, this area does not get depolarized. Filaments then can attach to this area after the field has been applied rather than the top, remaining I-shaped. Case success rates for this scheme were 0%, 35%, 0%, and 40% and its overall success rate was 20%.

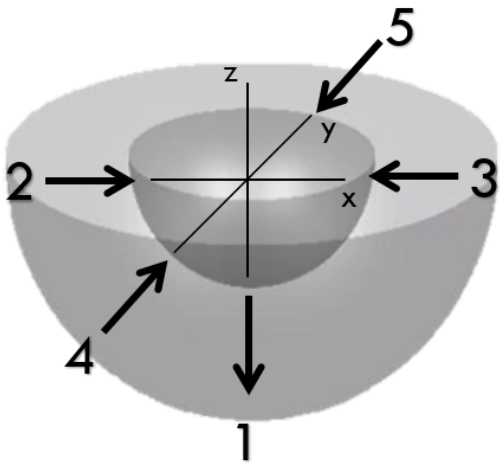

Figure 13: Order and directions in which electric fields in the "opposite" scheme were applied

IV.1.2 Electric Field Series: Opposite

Since the initial z direction field was not enough to cover the entire outside surface, we next tested the first series of five electric field pulses, referred to as "opposite". The fields applied in the x and y directions were applied in an attempt to cover the region around the top of the system. The order and direction in which each field was applied are as follows (see also Figure 13): negative z direction, positive x direction, negative x direction, positive y direction, and negative y direction. These fields were applied for 79 timesteps (2.528ms) with a 53 timestep (1.696ms) gap between them. Timing of fields should be such that a surface that is depolarized does not immediately get hyperpolarized, since this will cancel wave propagation. Likewise, if a surface is hyperpolarized and then depolarized soon after, no wave will form in that region due to its refractoriness. Because fields along the same axis are applied one after the next in this scheme, a gap is needed between fields to avoid the above mentioned problems. Case success rates for this method, shown in the second row of Figure 16, were 65%, 75%, 80%, and 85%. When the field was increased to 4.31 for one wave and 4.92 for three waves, all times tested were successful. The "opposite" scheme had an overall success rate of 90%. These success rates are much higher than both single stimulus schemes for each number of waves.

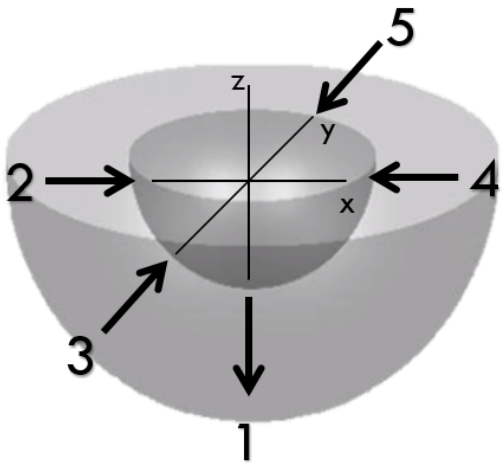

Figure 14: Order and directions in which electric fields in the "around" scheme were applied

IV.1.3 Electric Field Series: Around

While the above scheme had rather high success rates, another scheme utilizing five stimuli was tested in attempt to yield even better results. Electric fields applied in the "around" scheme, as seen in Figure 14, had the following order and direction: negative z direction, positive x direction, positive y direction, negative x direction, negative y direction. This scheme applied fields for 79 timesteps. However, since fields applied along the same axis are separated, no gap was needed between fields. Case success rates, shown in third row of Figure 16, here were 70%, 80%, 80%, and 95%. If the field was increased to 3.08 for three waves, there is complete success. In the case of two waves, no electric fields tested below the standard 5V/cm had complete success. The overall success rate for the "around" scheme was 90%. Success rates for each number of waves are in general higher than the previous "opposite" scheme and much higher than the single stimulus schemes.

IV.1.4 Sinusoidal Electric Field

Finally, we tested a sinusoidal scheme in a final attempt at defibrillation. This scheme was defined by a prolonged electric field applied with constant magnitude, but whose direction varied smoothly with time. The field, as seen in Figure 15, is described by:

$$E_x = E_{x_0}\sqrt{\frac{t}{d}}\cos\frac{2\pi t}{P} \tag{IV.1}$$

$$E_y = E_{y_0}\sqrt{\frac{t}{d}}\sin\frac{2\pi t}{P} \tag{IV.2}$$

$$E_z = E_{z_0}\sqrt{\frac{d-t}{d}} \tag{IV.3}$$

Here, t is the difference between the current timestep and the stimuli's beginning timestep, d is the stimulus duration, and P is the period. The sinusoidal scheme is similar to the behavior seen in the z direction scheme. Here, however, as time progresses the top of the system was depolarized. The field was applied for a total of 359 timesteps (11.488ms) with a period P of the same time. This period was chosen based on the same theory as the timing in the previous two schemes. Specifically, if the period is too short, cancellation happens as surfaces get both depolarized and hyperpolarized. On the other hand, if the period is too long, the entirety of the field is not applied, leaving a region which has not been depolarized. Results are shown in the last row of Figure 16. This scheme had case success rates of 40%, 30%, 50%, and 80% and an overall success rate of 55%. These results fall between the single stimulus schemes and the five stimuli schemes. Some explanation for why this might be the case is provided in the Discussion section.

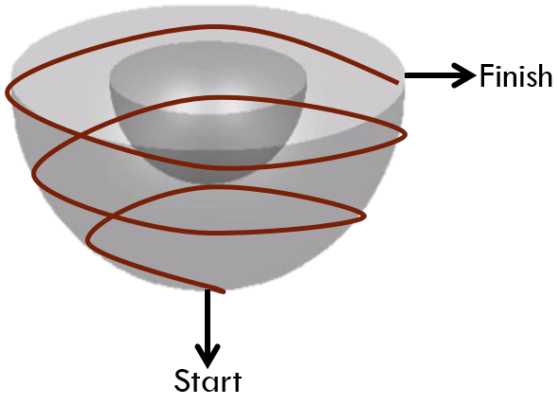

Figure 15: Motion of the tip of the electric field vector $\mathbf{E}_0$ as a function of time for the sinusoidal field scheme

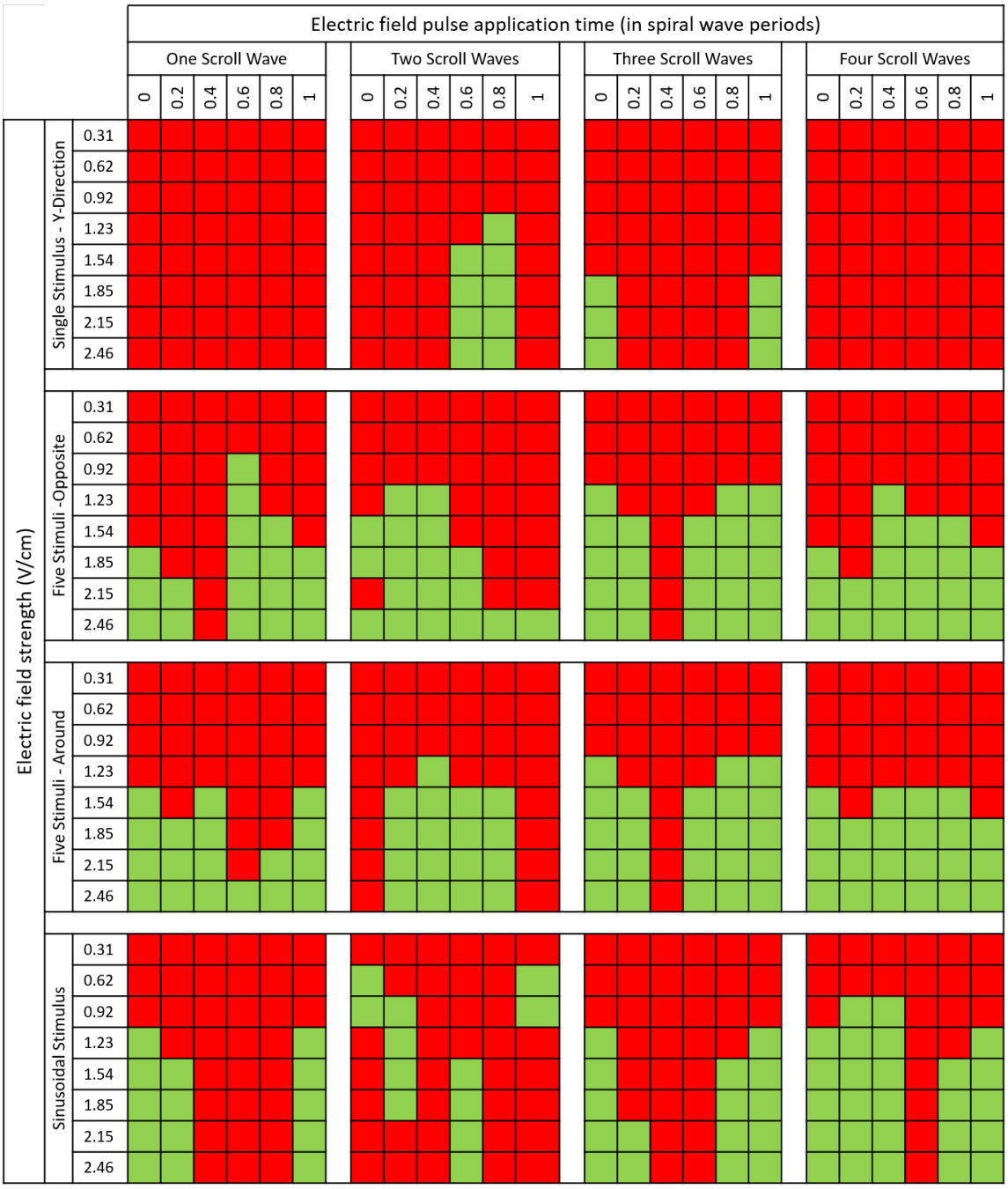

Figure 16: Results for computer simulations. Successful defibrillation is represented with green and unsuccessful with red.

V. Discussion

Our new schemes are all based on the idea of detaching filaments. First, as seen from the 3-D box simulations, filaments in the system contract [34], acting like rubber bands. Filaments that are I-shaped tend to persist indefinitely, but U- and C-shaped filaments tend to shrink and disappear. Second, we note that all scroll wave filaments that are attached to surfaces which are depolarized by an electric field pulse immediately detach from those surfaces. Third, we observe that if we can depolarize the entire outside surface of a hemispherical shell-shaped system (analogous to a ventricle-shaped system), all filaments detach from this surface. The resulting filaments, including all those that were originally I-shaped, would then necessarily become C-shaped or U-shaped. We would then expect all these filaments to shrink and disappear, resulting in termination of all the scroll waves.

Zemlin's description of the effects of electric fields on filaments is a little different. He believes that the hyperpolarized surface also disconnects the filament from the surface. While this may occur briefly in our model, the filament quickly reattaches to the surface. We also believe that it is not enough to use the filament shape after depolarization to predict the success of defibrillation. In our model, the filament orientation sometimes changes after the scroll wave has had time to rotate.

Figure 17 shows an example of this idea in action, in which three scroll waves are successfully extinguished. The top row shows both the waves and the filaments while the bottom only shows the filaments. We see the three scroll waves in column A. Column B shows the system while the series of pulses are being applied. During this time, the waves and filaments become complicated. We see that the fields have pushed the filaments off of the inside and outside walls so that they connect to the top. Note that the black- and blue-colored filaments here are plotting errors. They are either false filaments or falsely identified as being connected to a surface because of their proximity to it. After the series of fields has been applied, the waves settle down. In column C, these waves have settled into two scroll waves, one with a C-shaped filament and the other with a U-shaped one. Both of these filaments contract and eventually disappear. We see in column D that the C-shaped filament has already done so, leaving only the U-shaped which has greatly decreased in size. Soon after this, that filament also disappears.

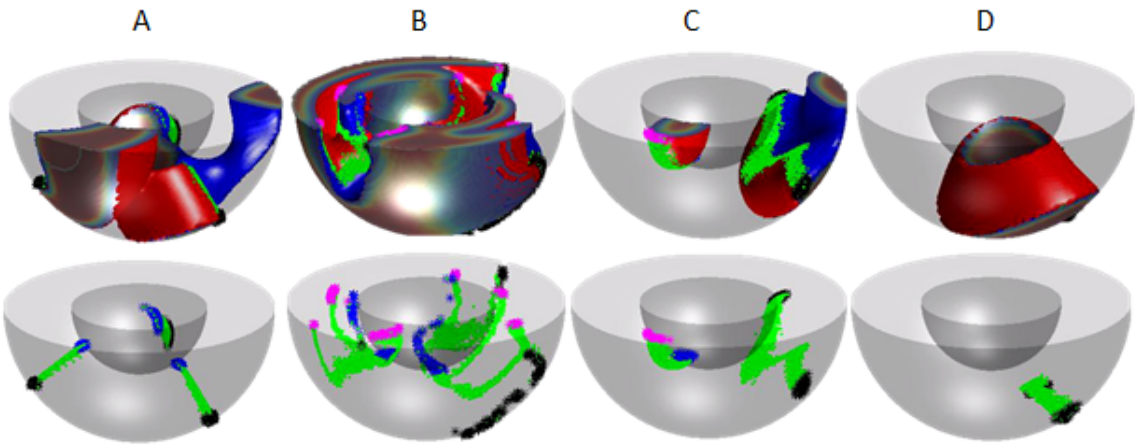

Figure 17: Successful termination of three waves using the "opposite" scheme with a strength of 1.85V/cm.

V.1 Five-Field Results Discussion

The electric field series schemes presented are successful independent of knowing: (1) the number of scroll waves present, (2) the location of those waves, (3) a wave's rotational phase, and (4) when the series of pulses is applied. Other attempts at terminating scroll waves, as mentioned in the "Previous Work" section, are generally limited by at least one of the things listed above.

We also find that both series of five electric fields work better than the standard single stimulus method. In all but one case, an electric field with strength less than the standard 5V/cm currently used for defibrillation results in complete success. For 90% of all wave number and time pairings, this field strength was less than half of the standard strength. 65% of pairings had successful termination at a strength of about 1.54V/cm, much less than the standard strength.

Both the "opposite" and "around" schemes have about the same success. While the "opposite" scheme had success rates which are slightly lower, every set of waves could be terminated with an electric field strength less than 5V/cm. On the other hand, the "around" scheme had a case, in the presence of two waves, for which there is a time that no field strength results in success. This scheme had overall higher success rates though, and overall required less strength to terminate scroll waves.

V.2 Sinusoidal Results Discussion

In general, this scheme best depolarized the entire outside surface of the system. Because of this, intuition suggests that it should have the best performance. However, this isn't the case. We believe that as the field is being applied, the hyperpolarization applied to the opposite side of the outer surface may be interfering with the preceding or subsequent depolarization of that surface. This formed a gap in which filaments could connect. Success rates for this scheme, then, were much lower than expected. We can see in some of the tables that there are orientations for which no electric field strength below 5V/cm resulted in successful defibrillation. There are other cases in which low field strengths successfully terminated waves, but higher strengths for the same waves did not. Further work with various periods and stimulus duration times may yield better results.

V.3 Failure Mechanisms

In cases where our method fails, we see specific patterns of behavior of the filaments. Failure occurs when the C- or U-shaped filaments return to an I-shaped filament. This happens when filaments get too close to either the inside or outside surface and reattach to that surface. We are still unsure of the exact mechanism that determines when a filament reattaches to a surface but believe it relates to the behavior seen in the rectangular system. That is, we believe the curvature of the wave greatly affects its ability to propagate when the filament is close to a surface, as described previously in the Building Concepts section.

The reformation of I-shaped filaments can happen in several ways. While there might be some cases not shown, we believe that most cases in which a filament reverts back to being I-shaped fall in one of the following four categories. In Figure 18, three waves are present; two I-shaped and one C-shaped. We see in the middle two plots that the top of the C-shaped filament becomes closer to the edge between the inside and top surfaces. This causes the filament to attach to the inside surface and become I-shaped. In the last plot, the newly formed I-shaped filament is slightly curved. This will continue to straighten, moving downward, until it resembles the other filaments.

C-shaped filaments can also cause termination failure when the ends of the filament are on opposite sides of the outer surface. As the filament contracts, as seen in Figure 19, the middle of the filament runs into the inner surface. Once this happens, two new filaments are formed: an

I-shaped and a C-shaped. The C-shaped will contract and disappear, provided it is far enough away from an edge. The I-shaped, seen in the last plot, will contract only to the point that it is straight and then will persist.

A similar failure happens when the C-shaped filament is connected on opposite sides of the inner surface with one end on that surface. As seen in Figure 20, this filament is very long and close to the outer surface. As the wave tries to propagate around the filament here, it does not have enough room and the filament connects to the surface. This results in a C-shaped filament and I-shaped filament being formed. In the simulation shown in Figure 20, the top of the C-shaped filament in the third plot attaches to the outside wall as described above and becomes U-shaped. In either case, the C- or U-shaped filaments disappear while the I-shaped filament(s) remain.

Finally, U-shaped filaments can cause failure in one of two ways. The first, shown in Figure 21, consists of a U-shaped filament connected to the outside surface. As seen in the first plot, the middle of the surface is close to the inner surface. Here, the wave does not have enough room to continue propagating, pulling the filament closer to the inner surface and attaching to it (plots 2 and 3). Once the middle attaches to the inner surface, two I-shaped filaments are formed. A similar cause of failure occurs if the U-shaped filament is attached to the inner surface. The middle of this filament can get too close to the outer surface and form two I-shaped filaments in the same way as described above.

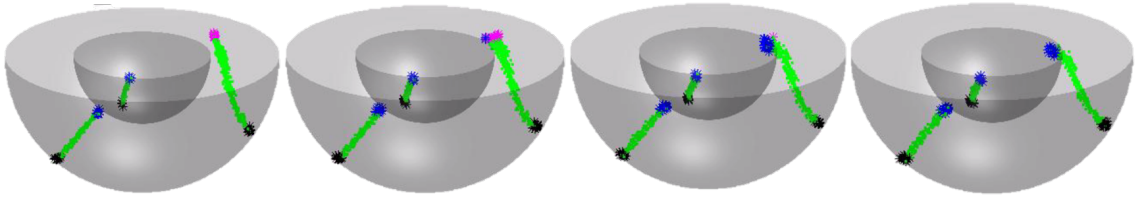

Figure 18: Failure to terminate caused by reconnection of top of filament

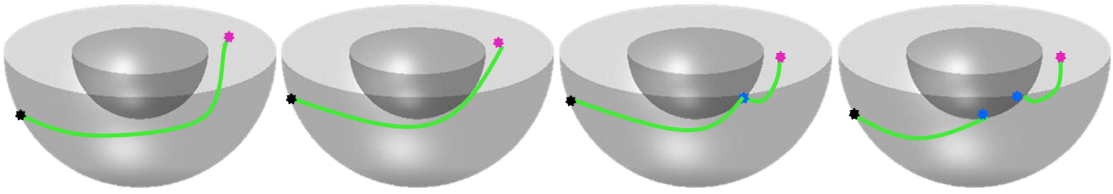

Figure 19: Failure to terminate caused by reconnection of middle of C-shaped filament to inside surface

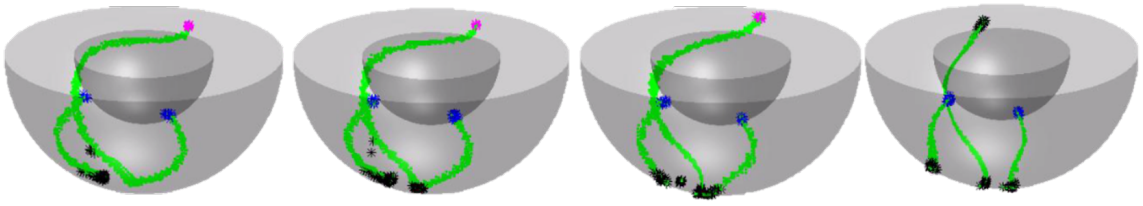

Figure 20: Failure to terminate caused by reconnection of middle of C-shaped filament to outside surface

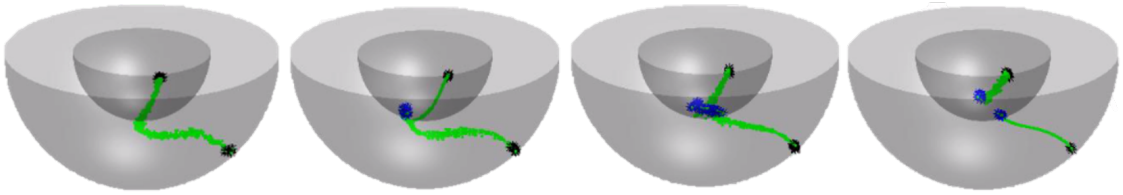

Figure 21: Failure caused by reconnection of middle of U-shaped filament to inside

V.4 Benefit of Reconnection

In the same way that the movement of a filament can cause termination of scroll waves to fail, it can also lead to the success of termination. Sometimes, a filament can change from I-shaped to C-shaped. This happens when one end of the filament gets close to the top surface. The curvature issue discussed before works in the favor of defibrillation here, causing the end to connect to the top surface. The newly formed C-shaped filament can then contract and disappear.

Interactions between filaments can also provide help with the termination of scroll waves. If the filaments of two waves get close together, they can reconnect. The waves must both be rotating with opposite chiralities for this to happen, however. A number of interactions between two filaments that are moving toward each other are shown in Figure 22. In many of these interactions, the resulting filaments are ones that will contract and disappear.

One of these interactions can be seen in Figure 23. In the simulation, an I-shaped and C-shaped filament have been formed following the application of an "opposite" series. We see in the second plot that they get close to each other. The extra green dots, while errors in the plotting of the filament, show how the filaments are getting pulled towards each other. Once they have connected, they break off into two new filaments; a U-shaped and C-shaped filament. The last plot shows these filaments as they begin to contract. In this case, an I-shaped filament, which would typically persist in the system and cause a failure, interacts with another filament to produce two filaments that eventually disappear.

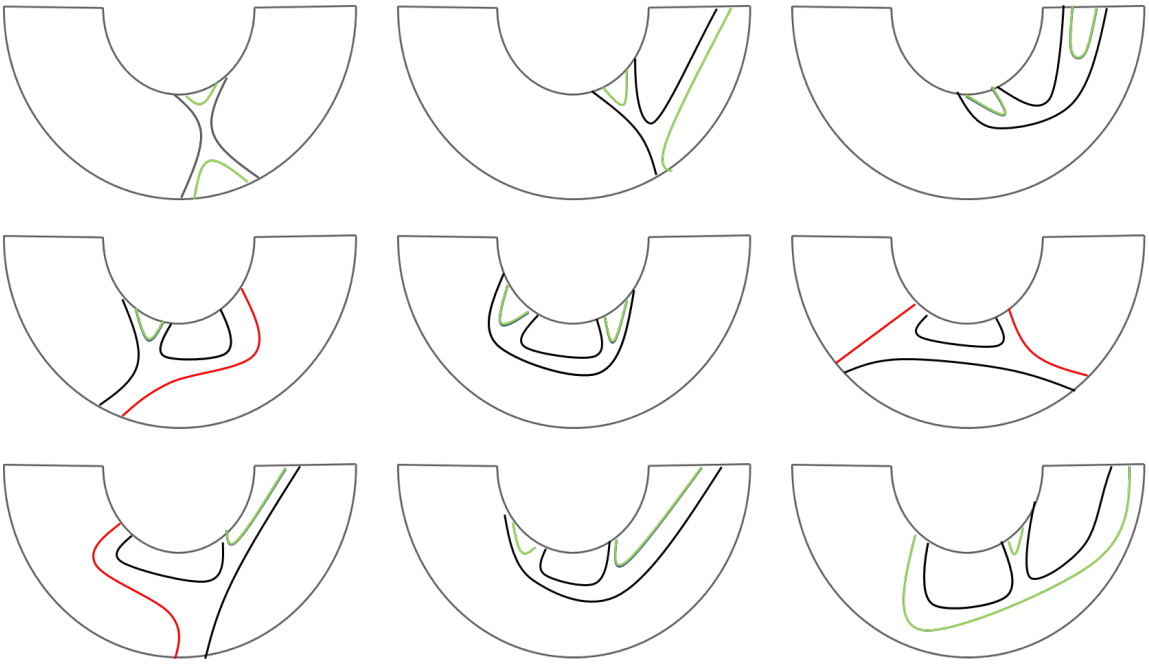

Figure 22: Some possible orientations of filaments and resultant filaments after reconnection. Black filaments are originals, red are I-shaped, and green are either U- or C-shaped.

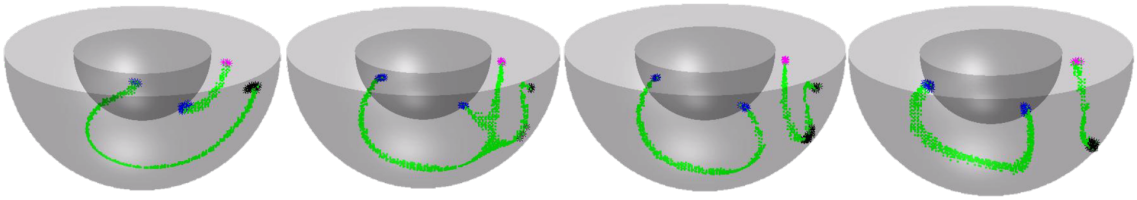

Figure 23: Interaction between an I-shaped and C-shaped filament

V.5 Second Series Results

Since there are cases in which the series of low-energy fields do not successfully terminate the scroll waves, we consider applying a second set of stimuli to the system. In this thesis, only one instance is tested. Specifically, we tested the case in which two waves have failed to be terminated after a series of electric fields in the "opposite" scheme has been applied. In this simulation, one wave remains after the initial series. The second set of fields were applied between one and ten wave periods after the last field in the first set and had strengths between 0.31 and 1.85V/cm, the strength of the initial fields. We see that this series was, in general, only successful for a field strength matching that of the initial series (1.85V/cm).

V.6 Limitations

A number of limitations with our model stem from the fact that it is a simplification of the heart and its properties. Our system only captures the basic geometry of the heart. We also assume that the tissue in our system is uniform and isotropic. In the heart, the fibers in the tissue may affect where the scroll waves occur, the direction they move, and their speed.

Another simplification made is in the use of the Barkley equations. These only depend on the membrane potential and the refractoriness of cells but do not consider other properties of the ion channels. These channels have complex behavior affecting a wave's ability to propagate. Additionally, we have chosen parameters for the Barkley model in the collapsing scroll wave regime. This means that our filaments have the nice behavior of contracting until they disappear. It is possible that, in an actual heart, filaments may acquire the tendency to expand, especially after prolonged fibrillation.

Our waves tend to have an action potential duration that doesn't vary much. In the real heart, there can exist alternans, a pattern of waves with alternating long and short action potential duration. In some cases, a wave gets so short that no action potential propagates. This leads to gaps in the waves which in turn create new waves.

Finally, a potential issue with the application of the second series of pulses is the possibility that applying this second set of fields could create new filaments or spiral waves. The timing of the second series might need to be narrowed down as well. As discussed by Zemlin in [23] and seen in our work, successful termination of scroll waves may be delayed. This means it might take time to determine whether the initial series of fields is successful before deciding to apply a second

series. Further work can be done in this area to determine this timing and to check the success of the second series of electric fields in all cases in which the initial series fails.

Despite these limitations, we believe that our model represents a promising method for low-energy propagation. Simplified models, like the Barkley model, provide new ideas about this topic. Specifically, this study provides us with new concepts of potential importance, such as the role played by the detaching of filaments using the fields, the creation of U- and C-shaped filaments, and the reasons why these mechanisms occasionally fail to produce defibrillation.

VI. Conclusions and Future Work

We present methods for applying a series of low-energy electric fields in different directions to a hemispherical shell system. These methods include a single electric field pulse, two different orientations of five electric field pulses, and a prolonged electric field pulse whose direction varies sinusoidally with time. These methods do not depend on knowledge of (1) the number of scroll waves present, (2) the location of those waves, (3) a wave's rotational phase, and (4) when the series of pulses is applied to be successful. The electric fields depolarize the outer surface of the system, detaching the filaments (around which the scroll waves rotate) from the surface. This causes the originally I-shaped filaments to become either C- or U-shaped. Filaments with the latter two orientations then tend to shrink and disappear. We find that both of the five electric field series work better than the standard single pulse. In most cases, we found that all filaments initially detached from the outside surface and then shrunk and disappeared. However, there were times that the filaments reconnected or reattached to adjoining surfaces, causing defibrillation to fail. Mechanism which cause this behavior are known.

There are several areas on which future work can focus. First, work can be done on improving existing schemes. Electric field duration and application times can be varied in an attempt to better cover the entirety of the outside surface. New schemes can also be created using the same basic principles used in this thesis. Next, work on the application of a second electric field series should be continued. Only one case has been tested thus far so the remaining cases should be tested to better understand the effects of the second set. Finally, improvements can be made to the model and system to make them more realistic. Some examples include the inclusion of ion channels, heterogeneities, and fiber direction and the use of a more life-like geometry (see Limitations section for more details).

Overall, we believe our new methods represent promising new ideas that will useful in future low-energy defibrillation research. In particular, insight can be gained about the behavior of filaments after the application of an electric field and their role in the success of low-energy defibrillation methods.

VII. Acknowledgments

I would first like to thank my advisor Dr. Niels Otani for his continuous support, feedback, guidance, and knowledge. When I approached him about research, I had very little knowledge of this field and I am grateful for all the work he has done helping me grow and learn.

I would also like to thank my thesis committee: Dr. Elizabeth Cherry and Dr. Laura Munoz, for their support and insightful comments. My sincere thanks also goes to Dr. Valentin Krinski and Dr. Vadim Biktashev for their valuable comments and insights on this project.

Finally, I would like to thank my loved ones for their support (and patience) throughout this whole process. This would not have been possible without them.

Kayleigh Wheeler
August 2017

VIII. Bibliography

References

[1] E. J. Benjamin, M. J. Blaha, S. E. Chiuve, M. Cushman, S. R. Das, R. Deo, S. D. de Ferranti, J. Floyd, M. Fornage, C. Gillespie, C. R. Isasi, M. C. Jiménez, L. C. Jordan, S. E. Judd, D. Lackland, J. H. Lichtman, L. Lisabeth, S. Liu, C. T. Longenecker, R. H. Mackey, K. Matsushita, D. Mozaffarian, M. E. Mussolino, K. Nasir, R. W. Neumar, L. Palaniappan, D. K. Pandey, R. R. Thiagarajan, M. J. Reeves, M. Ritchey, C. J. Rodriguez, G. A. Roth, W. D. Rosamond, C. Sasson, A. Towfighi, C. W. Tsao, M. B. Turner, S. S. Virani, J. H. Voeks, J. Z. Willey, J. T. Wilkins, J. H. Wu, H. M. Alger, S. S. Wong, and P. Muntner, "Heart disease and stroke statistics—2017 update: A report from the american heart association," *Circulation*, vol. 135, no. 10, pp. e146–e603, 2017.

[2] A. C. Guyton and J. E. Hall, *Textbook of Medical Physiology*. Elsevier Saunders, eleventh ed., 2006.

[3] F. H. Fenton, S. Luther, E. M. Cherry, N. F. Otani, V. Krinsky, A. Pumir, E. Bodenschatz, and R. F. G. Jr, "Termination of atrial fibrillation using pulsed low-energy far-field stimulation," *Circulation*, pp. 467–476, 2009.

[4] J. Keener and J. Sneyd, *Mathematical Physiology*, vol. 8. Springer, second ed., 2009.

[5] A. L. Hodgkin and A. F. Huxley, "A quantitative description of membrane current and its application to conduction and excitation in nerve," *J. Physiol.*, vol. 117, pp. 500–544, 1952.

[6] R. A. FitzHugh, "Impulses and physiological states in theoretical models of nerve membrane," *Biophys. J.*, vol. 1, pp. 445–466, 1961.

[7] J. Nagumo, S. Arimoto, and S. Yoshizawa, "An active pulse transmission line simulating nerve axon," *Proc. IRE*, vol. 50, pp. 2061–2070, 1962.

[8] M. E. Valentinuzzi, *Cardiac Fibrillation-Defibrillation: Clinical and Engineering Aspects*. World Scientific Publishing Company, 2010.

[9] D. Hornung, V. N. Biktashev, N. F. Otani, T. K. Shajahan, T. Baig, S. Berg, S. Han, V. I. Krinsky, and S. Luther, "Mechanisms of vortices termination in the cardiac muscle," *Royal Society Open Science*, February 2017.

[10] C. M. Ripplinger, V. L. Krinsky, V. P. Nikolski, and I. R. Efimov, "Mechanisms of unpinning and termination of ventricular tachycardia," *Am J Physiol Heart Circ Physiol*, pp. 184–192, 2 2006.

[11] S. Luther, F. H. Fenton, B. G. Kornreich, A. Squires, P. Bittihn, D. Hornung, M. Zabel, J. Flanders, A. Gladuli, , L. Campoy, E. M. Cherry, G. Luther, G. Hasenfuss, V. I. Krinsky, A. Pumir, R. F. Gilmour Jr., and E. Bodenschats, "Low-energy control of electrical turbulence in the heart," *Nature*, vol. 475, pp. 235–239, 7 2011.

[12] W. Li, C. M. Ripplinger, Q. Lou, and I. R. Efimov, "Multiple monophasic shocks improve electrotherapy ofventricular tachycardia in a rabbit model of chronic infarction," *Heart Rhythm*, vol. 6, pp. 1020–1027, 2009.

[13] C. M. Ambrosi, C. M. Ripplinger, I. R. Efimov, and V. V. Fedorov, "Termination of sustained atrial flutter and fibrillation using low voltage multiple shock therapy," *Heart Rhythm*, vol. 8, pp. 101–108, 2011.

[14] Y. C. Ji, I. Uzelac, N. Otani, S. Luther, R. F. Gilmour Jr., E. M. Cherry, and F. H. Fenton, "Synchronization as a mechanism for low-energy anti-fibrillation pacing," *Heart Rhythm*, vol. 14, pp. 1254–1262, 2017.

[15] K. H. ten Tusscher, D. Noble, P. J. Noble, and A. V. Panfilov, "A model for human ventricular tissue," *Am. J. Physiol. Heart Circ. Physiol.*, vol. 286, no. 4, pp. H1573–H1589, 2004.

[16] L. Priebe and D. J. Beucelmann, "Simulation study of cellular electric properties in heart failure," *Circ res*, vol. 82, pp. 1206–1223, 1998.

[17] A. Nygren, C. Fiset, L. Firek, J. W. Clark, D. S. Lindblad, R. B. Clark, and W. R. Giles, "Mathematical model of an adult human atrial cell: the role of K+ currents in repolarization," *Circulation Research*, vol. 82, pp. 63–81, 1998.

[18] T. O'Hara, L. Virag, A. Varro, and Y. Rudy, "Simulation of the undiseased human cardiac ventricular action potential: Model formulation and experimental validation," *PLoS Computational Biology*, vol. 7, 2011.

[19] C.-H. Luo and Y. Rudy, "A model of the ventricular cardiac action potential: depolarization, repolarization, and their interaction," *Circ. Res.*, vol. 68, pp. 1501–1526, 1991.

[20] C.-H. Luo and Y. Rudy, "A dynamic model of the cardiac ventricular action potential i. simulations of ionic currents and concentration changes," *Circ. Res.*, vol. 74, pp. 1071–1096, 1994.

[21] D. Barkley, M. Kness, and L. S. Tuckerman, "Spiral-wave dynamucs in a simple model of excitable media: The transition from simple to compound rotation," *Phys. Rev. A*, vol. 42, no. 4, pp. 2489–2492, 1990.

[22] D. Barkley, "Linear stability analysis of rotating spiral waves in excitable media," *Phys. Rev. Lett.*, vol. 68, no. 13, pp. 2090–2093, 1992.

[23] C. Zemlin, S. Mironov, and A. Pertsov, "Delayed success in termination of three-dimensional reentry:role of surface polarization," *Journal of Cardiovascular Electrophysiology*, vol. 14, no. 10, pp. S257–S263, 2003.

[24] J. Bragard, A. Simic, J. Elorza, R. O. Grigoriev, E. M. Cherry, R. F. Gilmour Jr., N. F. Otani, and F. H. Fenton, "Shock-induced termination of reentrant cardiac arrhythmias: Comparing monophasic and biphasic shock protocols," *Chaos*, vol. 23, 2013.

[25] N. F. Otani, "Termination of reentrant cardiac action potential propagation using far-field electrical pacing," *IEEE Transcations on Biomedical Engineering*, vol. 58, no. 7, pp. 2013–2022, 2011.

[26] N. Trayanova, J. Eason, and F. Aguel, "Computer simulations of cardiac defibrillation: a look inside the heart," *Computing and Visualization in Science*, vol. 4, pp. 259–270, 2001.

[27] N. A. Trayanova, B. J. Roth, and L. J. Malden, "The response of a spherical heart to a uniform electric field: A bidomain analysis of cardiac stimulation," *IEEE Transcations on Biomedical Engineering*, vol. 40, pp. 899–908, 1993.

[28] B. J. Roth and B. D. Langrill, "Approximate analytical solutions of the bidomain equations for electrical stimulation of cardiac tissue with curving fibers.," *Phys. Rev. E*, vol. 65, p. 051925, 2003.

[29] G. W. Beeler and H. Reuter, "Reconstruction of the action potential of ventricular myocardial fibres," *Journal of Physiology*, vol. 268, no. 1, pp. 177–210, 1977.

[30] V. N. Biktashev, *Evolution of vortices in active media*. PhD thesis, Moscow Institute of Physics and Technology, 1989.

[31] N. F. Otani, V. Krinsky, and S. Luther, "Three-dimensional electrical vortex termination in cardiac tissue: a solution to the problem of unknown rotational phase," *Phys. Rev. Lett.*, submitted.

[32] S. F. Alonso, S. and A. S. Mikhailov, "Taming winfree turbulence of scroll waves in excitable media," *Science*, vol. 299, March 2003.

[33] A. Pumir and V. Krinsky, "Unpinning of a rotating wave in cardiac muscle by an electric field," *J. theor. Biol*, pp. 311–319, 4 1999.

[34] J. P. Keener and J. J. Tyson, "The dynamics of scroll waves in excitable media," *SIAM Review*, vol. 34, pp. 1–39, March 1992.